The EMBO Journal Vol. 22 No. 3 pp. 502–514, 2003

Structural basis of adhesion-molecule recognition by ERM proteins revealed by the crystal structure of the radixin–ICAM-2 complex

Keisuke Hamada[1,2], Toshiyuki Shimizu[1,3], Shigenobu Yonemura[4,5], Shoichiro Tsukita[4], Sachiko Tsukita[4,6] and Toshio Hakoshima[1,7,8]

[1]Structural Biology Laboratory, Nara Institute of Science and Technology and [7]CREST, Japan Science and Technology Corporation, 8916-5 Takayama, Ikoma, Nara 630-0101, [4]Department of Cell Biology, Faculty of Medicine, Kyoto University, Sakyo-ku, Kyoto 606-8501 and [6]College of Medical Technology, Kyoto University, Sakyo-ku, Kyoto 606-8507, Japan

[2]Present address: RIKEN Harima Institute at SPring-8, 1-1-1 Kouto, Mikazuki-cho, Sayo-gun, Hyogo 679-5148, Japan
[3]Present address: Science of Biological Supramolecular Systems, Yokohama-city University, 1-7-29 Suehiro-cho, Tsurumi-ku, Yokohama, Kanagawa 230-0045, Japan
[5]Present address: RIKEN Center for Developmental Biology, 2-2-3 Minatojima-minami-machi, Chuo-ku, Kobe, Hyogo 650-0047, Japan

[8]Corresponding author
e-mail: hakosima@bs.aist-nara.ac.jp

ERM (ezrin/radixin/moesin) proteins recognize the cytoplasmic domains of adhesion molecules in the formation of the membrane-associated cytoskeleton. Here we report the crystal structure of the radixin FERM (4.1 and ERM) domain complexed with the ICAM-2 cytoplasmic peptide. The non-polar region of the ICAM-2 peptide contains the RxxTYxVxxA sequence motif to form a β-strand followed by a short 3_{10}-helix. It binds the groove of the phosphotyrosine-binding (PTB)-like subdomain C mediated by a β–β association and several side-chain interactions. The binding mode of the ICAM-2 peptide to the FERM domain is distinct from that of the NPxY motif-containing peptide binding to the canonical PTB domain. Mutation analyses based on the crystal structure reveal the determinant elements of recognition and provide the first insights into the physical link between adhesion molecules and ERM proteins.

Keywords: cell adhesion/cytoskeleton/recognition/signal transduction/X-ray

Introduction

In eukaryotic cells, actin filaments are concentrated in a layer beneath the plasma membrane called the cell cortex. Actin rearrangements within the cortex provide the molecular basis for changes in cell shape and for cell locomotion, cell adhesion and cell–cell communication. Cross-linker proteins that bind both membrane proteins and actin filaments mediate the formation of the membrane-associated cytoskeleton. One such protein is radixin, which is a member of ERM (ezrin/radixin/moesin) proteins localized at cell-surface structures such as microvilli, ruffling membranes and cell-adhesion sites (Sato *et al*., 1991, 1992; Franck *et al*., 1993; Amieva and Furthmayr, 1995; Serrador *et al*., 1997).

ERM proteins are close homologues with ~75% sequence identity (Arpin *et al*., 1994; Takeuchi *et al*., 1994; Bretscher, 1999; Mangeat *et al*., 1999; Tsukita and Yonemura, 1999) and have three domains: an N-terminal FERM (band 4.1 protein and ERM homology) domain consisting of ~300 residues (radixin residues 1–297), a central helical domain of ~200 residues (radixin 310–470) and a C-terminal tail domain of ~100 residues (radixin 477–583). The FERM domain of ERM proteins is responsible for binding to the cytoplasmic parts of adhesion molecules, while the C-terminal tail domain binds F-actin (Turunen *et al*., 1994). FERM domains have been found in several other proteins localized at plasma membranes (Chishti *et al*., 1998) and are currently thought to form a protein module to mediate protein–protein and protein–membrane interactions.

ERM proteins partition between the cell cortex and the cytosol. In the cytosol, ERM proteins exist as a masked form in which the FERM domain binds the C-terminal tail domain to mutually mask the binding sites for their binding partners (Andreoli *et al*., 1994; Magendantz *et al*., 1995; Gary and Bretcher, 1995; Hirao *et al*., 1996). This masked molecule is activated by the binding of phosphatidylinositol 4,5-bisphosphate (PIP2) to the FERM domain (Niggli *et al*., 1995; Hirao *et al*., 1996; Nakamura *et al*., 1999; Yonemura *et al*., 2002). Recent crystal structures of the radixin FERM domain complexed with the head group of PIP2, inositol-(1,4,5)-trisphosphate (IP3), have revealed that the IP3 binding induces local conformational changes in the FERM domain to release the C-terminal tail domain (Hamada *et al*., 2000). The unmasked state of ERM proteins is stabilized by phosphorylation of the C-terminal tail domain (reviewed by Tsukita and Yonemura, 1999; Bretscher *et al*., 2000).

To date, three adhesion molecules have been characterized as possible membrane partners of ERM proteins. These are a cell-surface hyaluronate receptor protein, CD44 (Tsukita *et al*., 1994; Serrador *et al*., 1997), a cell-surface glycoprotein of the sialomutin family, CD43 (Yonemura *et al*., 1993; Serrador *et al*., 1998) and the immunoglobulin-superfamily membrane proteins, ICAM-1 (Heiska *et al*., 1998), -2 (Helander *et al*., 1996; Heiska *et al*., 1998) and -3 (Serrador *et al*., 1997). These ICAMs mediate leukocyte and endothelial binding to β2-integrins. ICAM-1, -2 and -3 bind lymphocyte function-associated antigen-1 (LFA-1) via the N-terminal one or two immunoglobulin-fold domain(s), and ICAM-1 binds complement receptor 3/Mac-1 via the third immunoglobulin-fold domain. Thus, ICAMs do play an important role in cell–cell communication in the immune system.

How cross-linker proteins recognize adhesion molecules continues to be an area of intensive study. CD44

and CD43 have cytoplasmic domains consisting of 70 and 124 residues, respectively. In contrast, ICAMs have short cytoplasmic tail peptides as their cytoplasmic portions. For example, the mouse ICAM-2 tail consists of 28 residues. Recently, possible ERM-binding regions of CD43 and CD44 have been identified in their juxtamembrane regions consisting of 31 and 19 residues, respectively (Yonemura *et al*., 1998). All these regions contain repeated basic residues, although no significant sequence homology has been found. Interestingly, these positively charged regions are in sharp contrast with the highly negatively charged regions of cadherins for β-catenin binding (Huber and Weis, 2001). Because such a cluster of basic residues is a common feature of juxtamembrane regions of many adhesion molecules and receptors, it remains unclear how ERM proteins discriminate between them. Here, we report the first crystal structure of the FERM domain bound to the ICAM-2 cytoplasmic tail. The structure reveals how the FERM domain recognizes the cytoplasmic tail through interactions with subdomain C, which is folded into a phosphotyrosine-binding (PTB)-like domain, but exhibits a binding specificity distinct from canonical PTB domains.

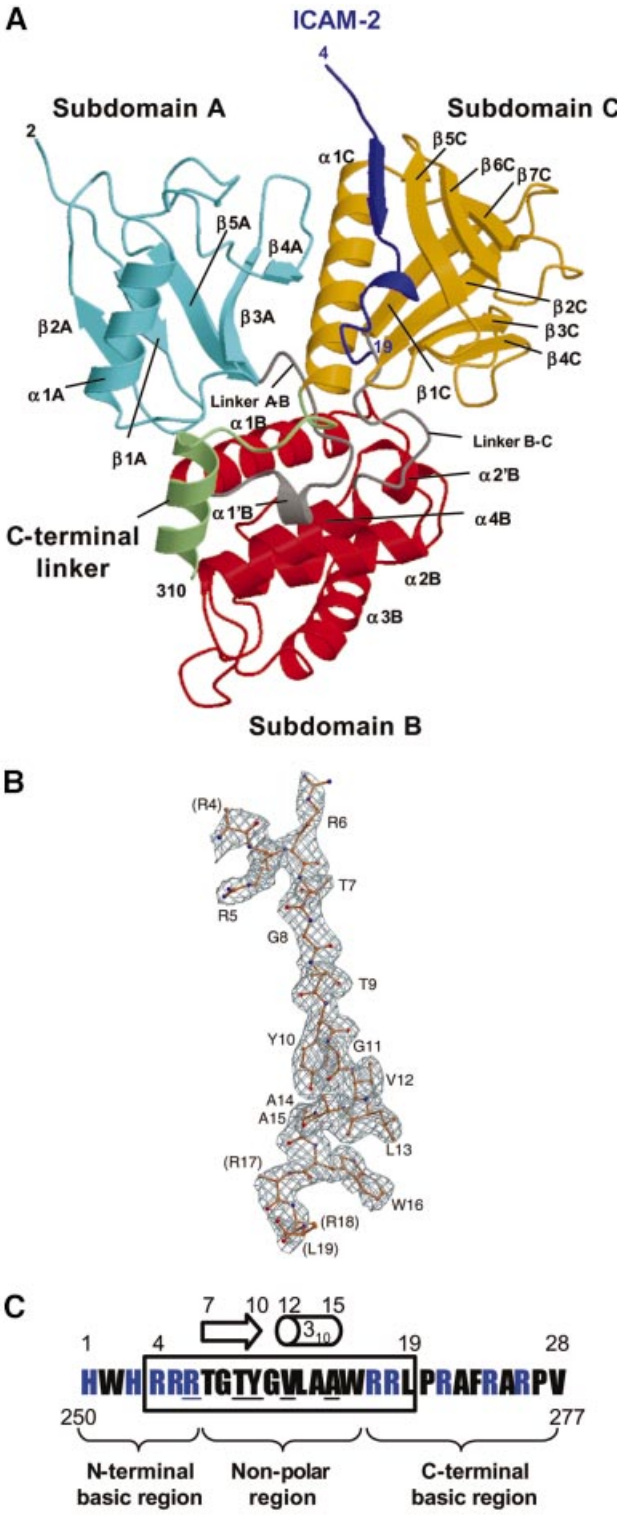

Results and discussion

Structure determination

The mouse radixin FERM domain containing residues 1–310 was purified as described (Hamada *et al*., 2001). The synthesized mouse ICAM-2 peptide is composed of 28 residues of the whole cytoplasmic tail (residues 250–277). Crystals of the radixin FERM domain bound to the ICAM-2 peptide containing one molecular complex per asymmetric unit were obtained. The structure was determined by molecular replacement using the free radixin FERM domain (Hamada *et al*., 2000) and refined to 2.4 Å resolution to an R value of 22.9% (a free R value of 24.0%). The current model includes 2–310 residues of the FERM domain and 16 residues (residues 4–19) of the ICAM-2 peptide, hereafter referred to as the FERM–ICAM-2 complex (Figure 1A). Most of the 16 residues are well defined on the electron density maps (Figure 1B). The numbering scheme of the ICAM-2 peptide is shown in Figure 1C. No model of the peptide was built for the three N-terminal residues (residues 1–3) and the nine C-terminal residues (residues 20–28), which were poorly defined in the current map, probably because of disordering.

Overall structure of the FERM domain

The radixin FERM domain contains three subdomains, A (the N-terminal 82 residues, light blue in Figure 1A), B (residues 96–195, red) and C (residues 204–297, brown). Subdomain A has a typical ubiquitin fold, and subdomain B has an α-helix bundle structure classified as an acyl-coenzyme A binding protein-like fold. Subdomain C folds into a standard seven-stranded β-sandwich with one long α-helix (α1C), classified as a PTB or pleckstrin-homology

Fig. 1. Overall structure of the radixin FERM domain bound to the ICAM-2 tail peptide. (**A**) Views of the radixin FERM domain bound to the ICAM-2 peptide by ribbon representations. The ICAM-2 peptide is shown in blue. The radixin FERM domain consists of subdomains A (light blue), B (red) and C (brown). The linkers A–B (residues 83–95) and B–C (residues 196–203) are colored in gray and the C-terminal linker in green. (**B**) The ICAM-2 peptide model in a $2F_o$–F_c electron density map countered at the 1σ level. The amino acid residues are indicated with labels of one-letter codes. Labels in parentheses indicate the terminal residues whose side chains were not defined in the map. (**C**) The 28-residue peptide synthesized based on the sequence of the mouse ICAM-2 cytoplasmic tail was used for the structural work. Basic residues are in blue. This peptide has two basic regions and a non-polar region between them. The 16 residues of the peptide defined on the current map are boxed. Key residues in binding to the radixin FERM domain are underlined (see text). The short β-strand (residues 7–10) and one 3_{10} helix (resides 12–15) are indicated with an arrow and a cylinder.

(PH) domain. These subdomain structures are essentially the same as those of the free and IP3-bound forms of the radixin FERM domain (Hamada *et al*., 2000). The average root mean square (r.m.s.) deviations in C_α atoms obtained from the pair-wise superposition of each subdomain in the ICAM-2- and the IP3-bound forms were found to be 0.58 Å, 0.86 Å and 0.89 Å for subdomains A, B and C, respectively. Subdomain B has a short flexible loop (residues 160–165) between helices α2′B and α3B displaying an exceptionally local deviation (~5 Å). In subdomain C, the C-terminal helix α1C moves toward the bound ICAM-2 peptide by 1 Å, which would be an induced fit by peptide binding. The C-terminal residues 298–310 (green in Figure 1A) of the current structure form a stable conformation, including an additional helix (residues 300–310). A proline residue Pro297 followed by helix α1C directs this segment to run along the interface between subdomain A and linker A–B.

The overall r.m.s. deviations of the ICAM-2 bound FERM domain from the free form are relatively large (1.35 Å), compared with the small deviations in each subdomain. In these global structural comparisons, the major deviation has been found to be due to subdomain A, which shifts its mutual position relative to subdomains B and C with a rotation of 3.5° around the A–B linker. The movement of helix α1C may trigger the movement of subdomain A, although the structure of the FERM–ICAM-2 complex does not preclude crystal-packing effects on subdomain A movement. The principal structural changes in the FERM domains described above are also seen in comparison with the moesin FERM–C-tail complex (Pearson *et al*., 2000), giving an average r.m.s. deviation

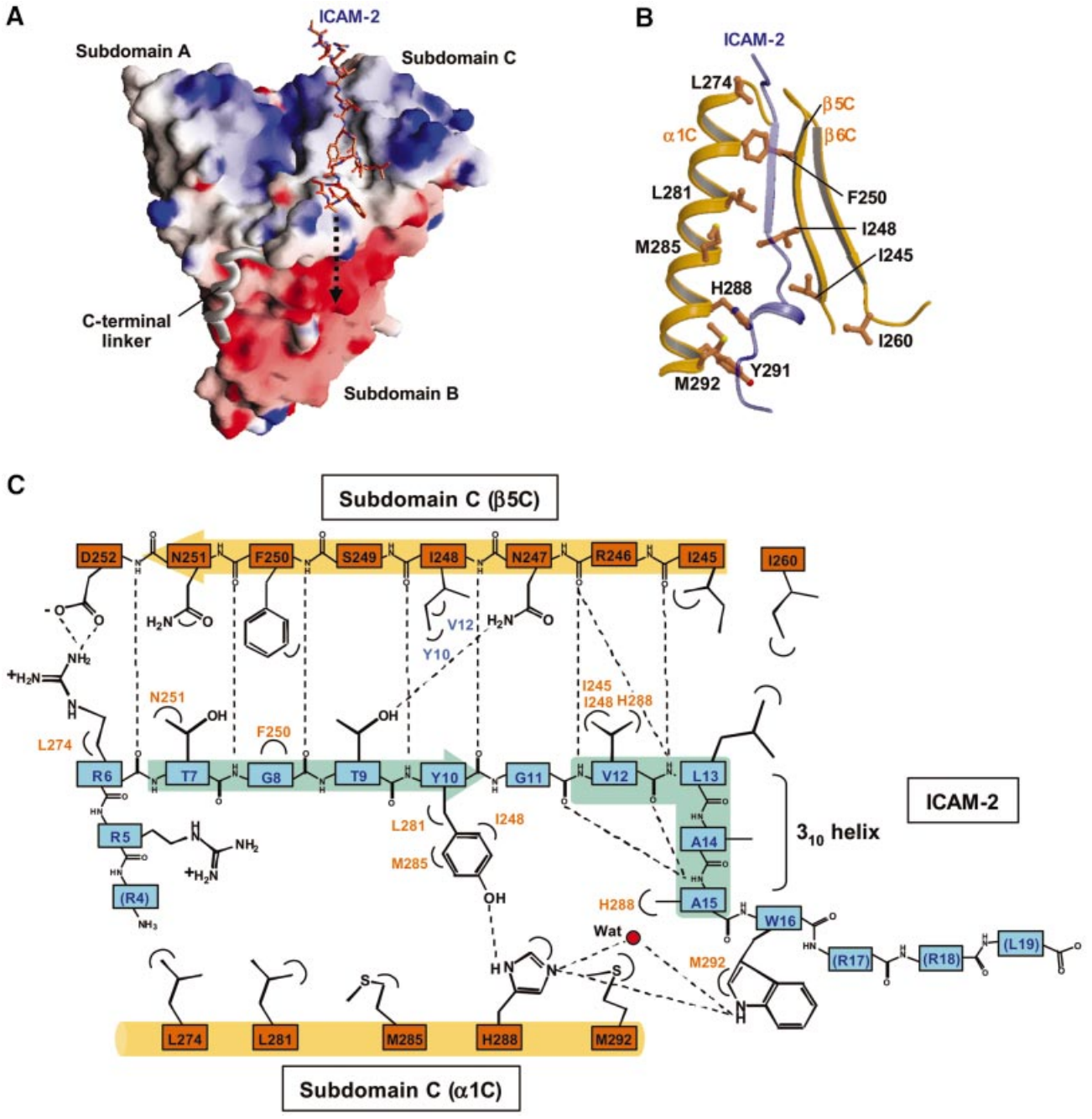

of 1.55 Å in C_α atom positions. One major difference producing this large deviation is the conformational differences in subdomains B and C, which contain the helix α2B and loop α2B–α2′B and β-sheet β5C–β6C–β7C. These differences are caused by induced fits upon binding to the C-terminal tail domain in the moesin complex, as discussed previously (Hamada *et al*., 2000).

Peptide structure and recognition

As shown in Figure 1C, the ICAM-2 peptide consists of three regions: the positively charged N-terminal and C-terminal regions separated by the non-polar region. Both the N-terminal and C-terminal regions are flexible, while the non-polar region forms a short β-strand (residues 7–10) followed by a short 3_{10} helix (residues 12–15). The structured peptide region fills a long shallow groove on the molecular surface of subdomain C (Figure 2A). This peptide-binding groove is formed by hydrophobic side chains from helix α1C and strand β5C (Figure 2B). Trp242 from loop β4C–β5C also participates in formation of the groove. Eleven residues (residues 6–16) of the ICAM-2 peptide are in contact with subdomain C and bury 1761 $Å^2$ of the total accessible surface area. The β-strand of the bound peptide forms an anti-parallel β–β association with strand β5C from subdomain C (Figure 2C). The binding mode of ICAM-2 to the FERM domain is comparable to those of phosphotyrosine-containing peptides bound to PTB domains, which will be discussed later. In our complex structure, eight main-chain–main-chain hydrogen bonds stabilize the ICAM-2 binding; five at the β-strand and three at the 3_{10} helix of the ICAM-2 peptide. These three hydrogen bonds contribute to stabilizing the short 3_{10} helix structure, along with two intra-molecular main-chain–main-chain hydrogen bonds (Figure 2C).

The ICAM-2 peptide contacts both polar and non-polar residues from strand β5C and helix α1C. The contacts contain hydrogen bonding, salt-bridging and hydrophobic interactions involving side chains, which together produce the specificity of the peptide binding (Figure 2C and D). Notably, a stretch of the non-polar residues (residues 10–16) of ICAM-2 peptide forms a compact fold with the short 3_{10}-helix and produces several contacts with the groove. Of these residues, Tyr10, Val12 and Ala15 insert their side chains deeply into the groove, allowing for intimate interactions with several non-polar residues from helix α1C and strand β5C. The well-conserved His288 residue (Figure 3A) from helix α1C is located at the center of the multiple contacts with the ICAM-2 residues and thereby seems to play a key role in stabilizing the peptide binding (Figure 2E).

Using surface plasmon resonance (SPR) measurements, we found that the mouse radixin FERM domain binds the ICAM-2 peptide with high affinity (16.4 nM), as shown in Table I. Based on our complex crystal structure, the binding affinity for several mutated or truncated ICAM-2 peptides was determined by the measurements. These measurements resulted in a weakening of the binding affinity to the FERM domain by 2- to 50-fold and allowed us to identify key residues of the peptide as discussed below.

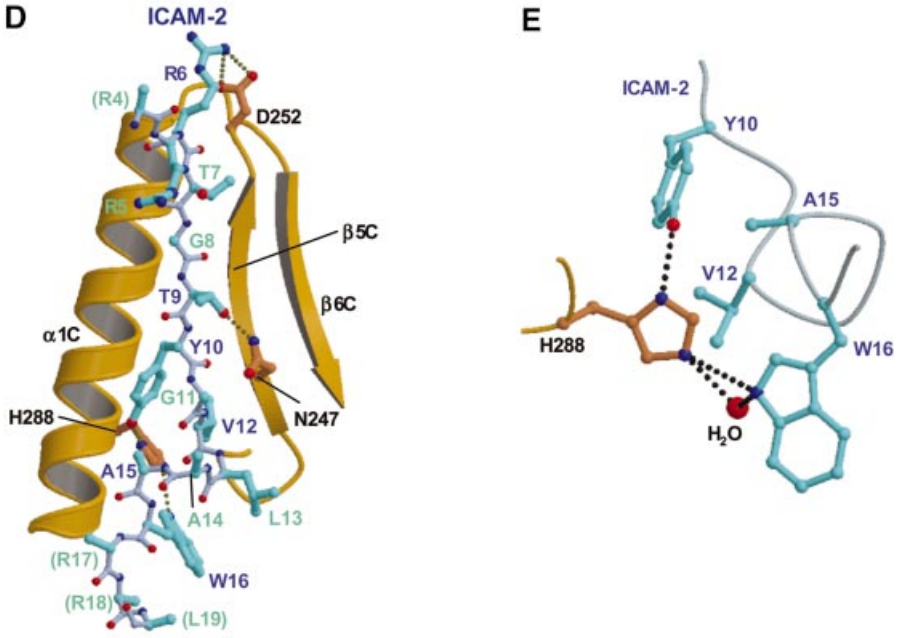

Fig. 2. The ICAM-2 tail peptide recognition by the radixin FERM domain. (**A**) Surface electrostatic potentials of the radixin FERM domain viewed from the same direction as in Figure 1A. Positive (blue, +14 kT/e) and negative (red, –14 kT/e) potentials are mapped on the van der Waals surfaces. The ICAM-2 peptide found in the complex crystal is shown in a stick model. The disordered C-terminal basic region is indicated by an arrow of dotted lines. (**B**) The ICAM-2 binding groove on subdomain C is formed primarily by hydrophobic residues from helix α1C and strand β5C. The bound ICAM-2 peptide is shown in a transparency ribbon model. (**C**) Schematic representation of the interactions between the ICAM-2 peptide (blue) and subdomain C (brown). Hydrogen bonds are shown by broken lines. (**D**) The ICAM-2 peptide found in the FERM–ICAM-2 complex is shown in a stick model (light blue) with their interacting residues from subdomain C (brown). Hydrogen bonds are shown by dotted lines. (**E**) A close-up view of the hydrophobic and hydrogen bonding interactions between the ICAM-2 peptide and the FERM domain mediated by His288 from subdomain C.

One determinant residue for the ICAM-2 binding specificity is Tyr10, which forms a hydrogen bond (2.7 Å) with His288 and is in contact with Ile248, Leu281 and Met285 from subdomain C. This Tyr residue is conserved in all ICAMs from different sources (Figure 3B), and the replacement with an Ala residue indeed significantly causes 16-fold reduction in the binding affinity (ICAM-2/Y10 in Table I). Val12 of the ICAM-2 peptide is conservative and is replaced with a Leu or Ile residue in some ICAMs, indicating the importance of its hydrophobic properties in binding to subdomain C. Leu13 is variant, contacting Ile260 from subdomain C at

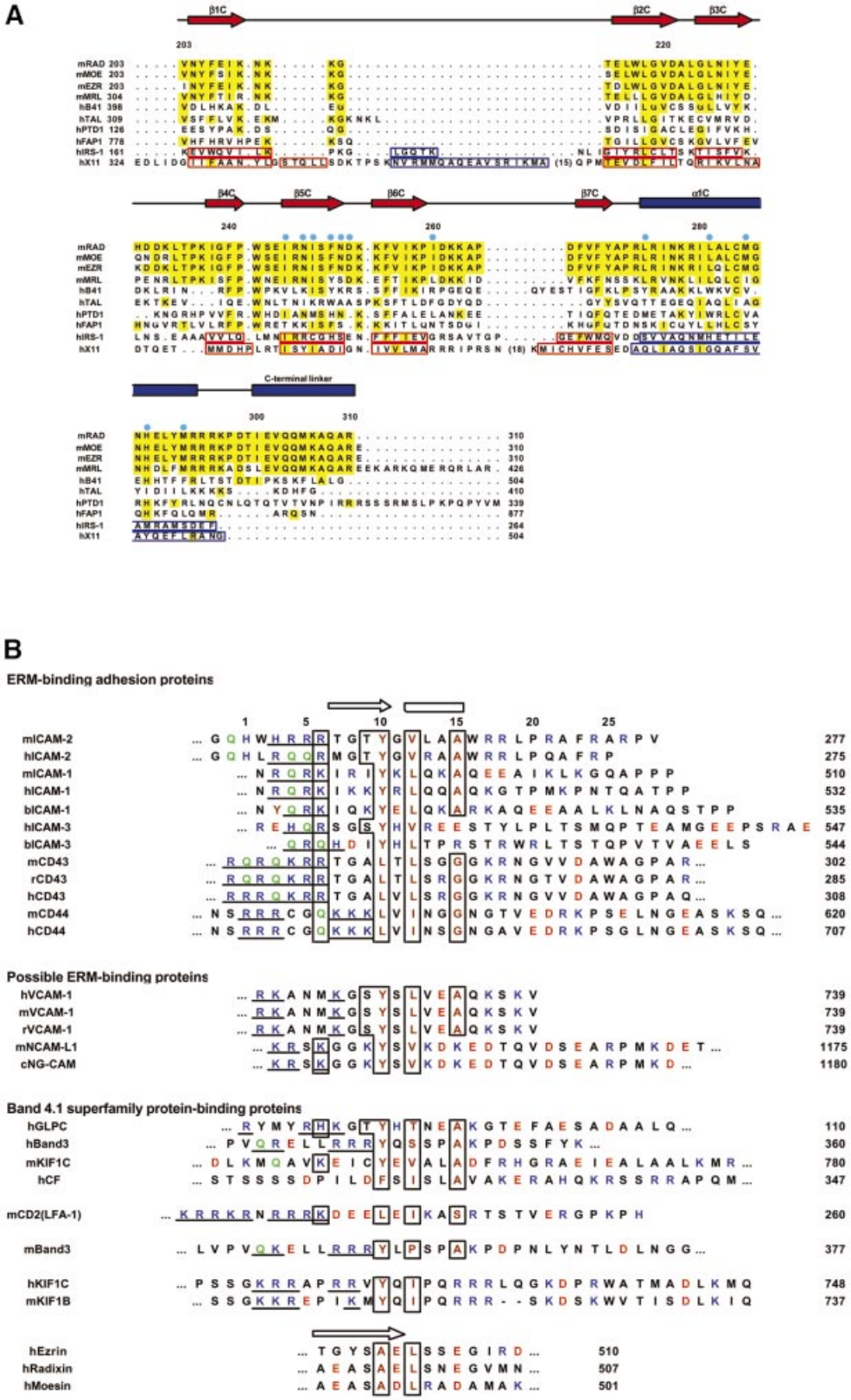

the molecular surface. A double mutation of Val12 and Leu13 by Ala reduces the binding affinity by 11-fold (ICAM-2/VL12 in Table I).

Trp16 of the ICAM-2 peptide also formed a possibly direct hydrogen bond (3.5 Å) as well as water-mediated hydrogen bonds with His288, although a single mutation of Trp16 by Ala was found to reduce the binding affinity by only two-fold (ICAM-2/W16 in Table I). This unexpectedly small contribution may be explained by Trp16 being rather bare at the molecular surface. Trp16 is conserved in ICAM-2 but is variant in other ICAMs, CD43 and CD44 (Figure 3B). Regarding the ICAM-2 arginine triplet at the N-terminal region, Arg6 forms a salt bridge (3.5 Å) with Asp252 from the C-terminal end of strand β5C (Figure 2D). Thr9 of the ICAM-2 β-strand forms a hydrogen bond (3.0 Å) to Asn247 of FERM strand β5C. Each substitution of Arg6 or Thr9 with Ala results in a weak reduction in the binding affinity (ICAM-2/R6 and ICAM-2/T9 in Table I).

In conclusion, we suggest a FERM-binding motif, RxxTYxVxxA (x stands for any amino acid residue), for ERM proteins. The key elements in the motif are Y, V and A, which play a central role in hydrophobic interactions with the FERM domain. In FERM-binding peptides from several sources, the Y and V positions are restricted to hydrophobic residues and the A position to small residues (Figure 3B). Two polar residues, R and T, in the motif have some significance in binding by participating in direct contacts with the FERM domain. The RxxTYxVxxA motif of ICAM-2 is followed by the C-terminal basic region, which is important for the strong binding as described in the next section.

C-terminal specificity

The C-terminal region of the ICAM-2 peptide is highly positively charged with five Arg residues (Figure 1C). In our complex structure, this flexible C-terminal region exhibits no specific interactions in terms of structure, but projects toward the highly negatively charged groove between subdomains B and C (Figure 2A). This shallow groove has been postulated as a possible site of interaction with the basic residues of the cytoplasmic tails of the FERM-binding adhesion molecules (Hamada *et al*., 2000). In fact, deletion of this region reduces the binding affinity to the FERM domain by 9-fold (ICAM-2/s2 in Table I). It is thus conceivable that this region electrostatically interacts with the acidic groove. This interaction provides a rational reason why the FERM binding to ICAM-2 was sensitive to ionic strength (Yonemura *et al*., 1998).

FERM binding to other adhesion molecules

Recently, ERM-dependent movement of CD43 distal to the T cell/APC (antigen-presenting cell) interaction sites has been shown to be an essential process for formation of the immunological synapse (Allenspach *et al*., 2001; Delon *et al*., 2001; Shaw, 2001). We found that the FERM domain binds the CD43 peptide with a K_d value of 104 nM (Table II). The CD43 peptide has Leu and Gly residues at positions corresponding to Tyr10 and Ala15 of the ICAM-2 peptide, respectively. This fact suggests that Tyr and Ala residues at this position are not necessarily a prerequisite for FERM binding and are replaceable by residues with similar properties. Moreover, Thr9 is replaced with an Ala residue. These replacements of the key residues are also seen in the CD44 peptide and may be one reason why the affinities of the CD43 and CD44 peptides are weaker than that of the ICAM-2 peptide. The ICAM-3 peptide exhibits an unexpectedly lower affinity (K_d value of 757 nM). In the ICAM-3 peptide, Ala15 of ICAM-2 is replaced with non-homologous residues and the C-terminal region lacks basic residues (Figure 3B). These possibly reduce the affinity to the FERM domain.

The observed binding affinities of ICAMs, CD43 and CD44 are basically consistent with previous results from an *in vitro* glutathione *S*-transferase (GST) pull-down binding assay and SPR measurements (Hirao *et al*., 1996; Heiska *et al*., 1998; Yonemura *et al*., 1998). A positive correlation between the isoelectric points of the cytoplasmic tail peptides and their binding affinity to ERM proteins has been pointed out previously (Yonemura *et al*., 1998). We found no significant binding affinity to ICAM-4 and ICAM-5 (data not shown).

Interestingly, we found that a short cytoplasmic peptide from the vascular cell adhesion molecule 1 (VCAM-1) possesses a region somewhat similar to the FERM-recognition motif of ICAM-2. This VCAM-1 peptide lacks the long C-terminal basic region, while our SPR measurements revealed a significant affinity (149 nM) of this VCAM-1 peptide for the FERM domain. It is likely that the basic residues close to the RxxTYxVxxA motif sequence are more important for the electrostatic interactions than remote basic residues at the C-terminal region. We also found that the neural cell adhesion molecule L1 (NCAM-L1), which shows limited sequence similarity, exhibits a relatively high affinity (61 nM). The affinities of these two newly found adhesion molecules for the radixin FERM domain are stronger than that of ICAM-3. It is noteworthy that recent biochemical studies have shown dynamic interaction of VCAM-1 with ERM

Fig. 3. Sequence alignments of subdomain C and the FERM-binding peptides. (**A**) Secondary structure elements and sequence alignments of subdomains C of FERM domains with the related PTB domains. The FERM subdomain C of mouse radixin (mRAD) and the related proteins are aligned with the secondary structure elements of the radixin FERM subdomain C at the top: α-helix (blue rectangles) and β-strands (red arrows). Identical residues are highlighted in yellow. The aligned FERM subdomains C are mouse radixin (mRAD), moesin (mMOE), ezrin (mEZR), merlin (mMRL), human band 4.1 (hB41), talin (hTAL), protein tyrosine phosphatase D1 (hPTPD1) and Fas-associated protein tyrosine phosphatase 1 (hFAP1). The aligned PTB domains are the IRS-1 PTB domain (hIRS1), the X11 PTB domain (hX11). The secondary structure elements of these PTB domains are boxed with blue lines (α-helices) and with red lines (β-strands). The mouse FERM domains exhibit 100% identities with those of human and >99.7% identities with other mammalian homologues. Blue circles mark the radixin subdomain C residues interacting with the ICAM-2 peptide. (**B**) Sequence alignment of the juxtamembrane cytoplasmic regions of adhesion molecules that bind ERM proteins and of the related adhesion molecules. Basic and acidic residues are shown in blue and red, respectively. The basic clusters located at the N-terminal region are underlined. Glutamines frequently appearing in this N-terminal basic region are shown in green. Key residues of the ICAM-2 peptide for binding to the radixin FERM domain are boxed with hydrophobic residues in brown. The sources are mouse (m), rat (r), human (h), bovine (b) and nematode (c). The numbers on the right-hand side of the column indicate the C-terminal residue numbers in the sequences. The N-terminal regions of the C-terminal tail domains of ERM proteins are also aligned at the bottom of the figure with an arrow indicating strand 1.

Table I. Binding affinities of the ICAM-2 peptides for the radixin FERM domain

Peptide[a]	Sequence[b]	K_d (nM)[c]	Fold reduction[d]
	1 ββββ hhhh 28		
xtal/visible	---RRRTGTYGVLAAWRRL---------		
ICAM-2	HWHRRRTGTYGVLAAWRRLPRAFRARPV	16.4 ± 1.4	1
ICAM-2/RR	**A**W**AAA**RTGTYGVLAAWRRLPRAFRARPV	31.5 ± 1.4	1/1.9
ICAM-2/R6	HWHRR**A**TGTYGVLAAWRRLPRAFRARPV	33.1 ± 1.8	1/2
ICAM-2/T9	HWHRRRTG**A**YGVLAAWRRLPRAFRARPV	33.1 ± 1.1	1/2
ICAM-2/W16	HWHRRRTGTYGVLAA**A**RRLPRAFRARPV	36.5 ± 0.1	1/2.2
ICAM-2/s2	HWHRRRTGTYGVLAAW	144.0 ± 11	1/9
ICAM-2/VL12	HWHRRRTGTYG**AAA**AWRRLPRAFRARPV	185.0 ± 51	1/11
ICAM-2/Y10	HWHRRRTGT**A**GVLAAWRRLPRAFRARPV	264.0 ± 37	1/16
ICAM-2/all	HWHRR**A**TG**AA**GVLAA**A**RRLPRAFRARPV	825.0 ± 11	1/50

[a]The peptides are for the juxtamembrane regions of mouse ICAM-2 (residues 250–277) and its mutation and deletion peptides. Mutated alanine residues in the ICAM-2 peptides are shown in bold.
[b]Residues characteristic in the FERM-binding peptides are boxed. The secondary structures, β-strand and 3_{10} helix, of the ICAM-2 peptide in our complex structure are indicated by β and h at the top.
[c]The obtained K_d values with their standard deviations. All measurements were performed at 25°C in HBP buffer containing 10 mM HEPES-Na (pH 7.4), 150 mM NaCl, 1 mM EDTA, 1 mM DTT and 0.05% surfactant P20.
[d]Fold reduction in relative affinity based on K_d values.

proteins in a novel endothelial docking structure for adherent leukocytes (Barreiro *et al*., 2002) and also functional binding of the axonal NCAM-L1 to ERM proteins (Dickson *et al*., 2002).

We notice that the FERM-binding motif proposed in this study resembles the juxtamembrane regions of syndecans and neurexins. Syndecans are heparan sulfate proteoglycans expressed on all adherent cells and participate in cell–cell, cell–matrix adhesion and signaling of heparan sulfate growth factors. Neurexins are brain-specific cell surface proteins, which bind neuroligins and neurexophilins, brain-specific adhesion molecules and neuropeptide-like molecules, respectively. We found that the radixin FERM domain binds syndecans and neurexin with relatively low affinities as compared with that of ICAM-2 (Table II). Syndecans and neurexins are known to have PDZ-binding sequences at their C-terminal ends, which bind PDZ-containing adaptor proteins, syntenin and CASK, respectively. In cells, these adaptor proteins may enhance the binding of syndecans and neurexins to ERM proteins. It is also possible that the binding partners of syndecans and neurexins in cells are the other members of ERM proteins or other FERM-containing proteins. We need further experimental tests to answer these questions.

Membrane targeting and unmasking

The N-terminal region of the ICAM-2 peptide contains five basic residues, His1 and 3, and Arg4–6 (Figure 1C). In our structure, this region is flexible. No direct interaction with the FERM domain is observed for these basic residues other than Arg6. This lack of direct interaction seems consistent with substitution of these basic residues with Ala (ICAM-2/RR in Table I) resulting in a weak 2-fold reduction of the binding affinity. A comparison of the FERM–ICAM-2 and FERM–IP3 complex structures reveals that these Arg residues are close to the bound IP3 molecule in the FERM–IP3 complex, but produce no direct contact with the IP3 molecule in the superimposed structures. Recently, several mutations have been introduced to ezrin to analyze the PIP2-binding site (Barret *et al*., 2000). It has been shown that mutations of basic residues at the membrane-binding surface of the FERM domain impair the PIP2 binding, while these mutations do not impair the *in vitro* interaction with the cytoplasmic tail of CD44. This result may be interpreted by our crystal structures, in which two binding sites for IP3 and ICAM-2 have no overlap as described above.

Recent SPR measurements suggest that PIP2 interacts with the ICAM-1 and -2 cytoplasmic tail peptides (Heiska *et al*., 1998). It seems plausible that in plasma membranes, negatively charged PIP2 molecules colocalize with ICAM-2 and other adhesion molecules having positively charged juxtamembrane regions of the cytoplasmic tails by electrostatic interactions. PIP2 molecules colocalized with adhesion molecules may recruit masked ERM proteins from the cytosol to plasma membranes and unmask ERM proteins for subsequent binding to the cytoplasmic tails of adhesion molecules (Figure 4A).

The C-terminal tail domain of moesin has been found to mask the acidic groove between subdomains B and C (Pearson *et al*., 2000), indicating that the C-terminal tail domain in masked full-length ERM proteins blocks the electrostatic interactions between the C-terminal basic region of the ICAM-2 peptide and the acidic groove of the FERM domain. Moreover, the N-terminal region (strand 1) of the C-terminal tail domain has been suggested to bind the groove of subdomain C, the place at which the ICAM-2 peptide was bound in our complex crystal. As shown in Figure 4B, this proposed binding in the masked full-length ERM proteins would directly interfere with binding of the ICAM-2 peptide to the FERM domain, although the sequence homology between the ICAM-2 strand and strand 1 of the C-terminal tail domain is not apparent (Figure 3B). A structure-based comparison indicates Tyr10 of ICAM-2, a key residue for binding, is replaced with Ala492 of the C-terminal tail domain (Figure 4C). In addition to the direct interferences described above, it should be noted that the overall structures of the FERM domains in the ICAM-2-bound and the masked forms show local structural deviations at subdomains B and C, as indicated previously. These deviations cause atom crashes

Table II. Binding affinities of the ICAM-2-related peptides for the radixin FERM domain

Peptide[a]	Sequence[b]	K_d (nM)[c]	Fold reduction[d]
ICAM-2/xtal	---RRRTGTYGVLAAWRRL---------		
ICAM-2	HWHRRRTGTYGVLAAWRRLPRAFRARPV	16.4 ± 1.4	1
NCAM-L1	IKRSKGGKYSVKDKEDTQVDSEARPMKDET	61.0 ± 19	1/3.7
ICAM-1	NRQRKIRIYKLQKAQEEAIKLKGQAPPP	68.0 ± 8.3	1/4.2
CD44	NSRRRCGQKKKLVINGGNGTVEDRKPSELNGEASKSQ	73.8 ± 4.1	1/4.5
CD43	RQRQKRRTGALTLSGGGKRNGVVDAWAGPAR	104 ± 7.2	1/6.3
VCAM-1	ARKANMKGSYSLVEAQKSKV	149 ± 28	1/9.1
ICAM-3	REHQRSGSYHVREESTYLPLTSMQPTEAMGEEPSRAE	757 ± 105	1/46
SDC-1	RMKKKDEGSYSLEEPKQANGGAYQKPTKQEEFYA	829 ± 338	1/51
SDC-4	RMKKKDEGSYDLGKKPIYKKAPTNEFYA	955 ± 210	1/58
NRX-1α	YKYRNRDEGSYHVDESRNYISNSAQSNGAV	3830 ± 850	1/234

[a]The peptides are for the juxtamembrane regions of ICAM-2 (residues 250–277), ICAM-1 (483–510), ICAM-3 (511–547), CD43 (272–302), CD44 (584–620), VCAM-1 (720–739), NCAM-L1 (1146–1175). All the sequences are from mouse proteins, but ICAM-3 is from human. SDC-1, -4 and NRX-1α are human syndecans-1 (277–310), -2 (1448–1477) and neurexin-1α (1423–1452), respectively.
[b]Characteristic residues in the FERM-binding peptides are boxed. Basic residues in the peptides are underlined.
[c]The obtained K_d values with their standard deviations.
[d]Fold reduction in relative affinity based on K_d values.

at the interfaces between the C-terminal tail domain and subdomains B and C, when the tail domain is overlaid on the FERM–ICAM-2 complex (Figure 4B).

Comparison with the phosphotyrosine-containing peptide bound to PTB domains

A previous structural comparison (Hamada *et al*., 2000) has indicated that the fold of subdomain C resembles the PTB domains rather than PH domains. The β-strand of the bound ICAM-2 peptide is superimposable onto that of the phosphotyrosine-containing peptide (pY peptide) from human insulin receptor (IR) bound to the human insulin receptor substrate 1 (IRS-1) PTB domain (Eck *et al*., 1996) (Figure 5A). The IR and other PTB-binding peptides have NPxY motifs (Figure 5B), which adopt a β-turn conformation at the C-terminal end of the β-strand. The ICAM-2 peptide, however, has no NPxY motif and the region corresponding to this NPxY motif forms a 3_{10} helix followed by the C-terminal region running in a direction different from that of the IR peptide (Figure 5C).

Compared with the pY peptide binding to PTB domains in a μM range of K_d (Dhe-Paganon *et al*., 1999), the ICAM-2 binding to the FERM domain is stronger by ~100-fold. There is, however, no significant difference in their buried accessible surface area at the interfaces, where the peptides have ordered structures. For example, the total buried accessible surface area in the complex between the IR peptide and the IRS-1 PTB domain is ~1560 Å^2 (Eck *et al*., 1996). The relatively stronger binding of the ICAM-2 peptide to the FERM domain may be attributable to possible electrostatic interactions between the C-terminal basic residues and the highly negatively charged groove between subdomains B and C. Another possible reason for the stronger binding of the ICAM-2 peptide may be attributable to differences in the main-chain–main-chain interactions. Eight main-chain–main-chain hydrogen bonds are formed in the FERM–ICAM-2 complex, whereas five are formed between the IR peptide and the IRS-1 PTB domain. In addition, lack of hydrophobic interactions involving the critical Y residue from the RxxTYxVxxA motif in the IR peptide could also explain the differences in binding affinity.

Interestingly, the neuron-specific X11 PTB domain has been shown to bind a non-pY peptide from β-amyloid precursor protein (APP) (Zhang *et al*., 1997). Another class of PTB domains, which contains the Numb PTB domain, binds peptides having a GPpY but not NPxpY motif (Li *et al*., 1998). The current structure provides new evidence that PTB domains have multiple modes of peptide binding with different specificities.

Comparison with β-catenin

It is an interesting question as to what relationship there is between recognition of the cytoplasmic peptides of adhesion molecules for linking the actin cytoskeleton by ERM proteins and other linker proteins. In the β-catenin–E-cadherin complex (Huber and Weis, 2001), the interaction surface involves 100 residues of the E-cadherin peptide, which has an extended structure at the long groove formed by the α-helical armadillo repeats of β-catenin. The cadherin peptide has polar and non-polar interactions with β-catenin primarily mediated by the side chains and raises the total buried accessible surface area of 6100 Å^2. No similarity of the peptide conformations and binding modes has been found between our FERM–ICAM-2 and the β-catenin–E-cadherin complexes. Notably, there is no main-chain–main-chain interaction between β-catenin and the E-cadherin peptide. It remains a mystery as to why the ICAM-2 binding affinity to the FERM domain is 14-fold stronger than the binding affinity of cadherin to β-catenin (230 nM), although the total buried accessible surface area in the FERM–ICAM-2 complex is 3.5-fold smaller than that in the β-catenin–E-cadherin complex. A lack of main-chain–main-chain interactions in the peptide binding to β-catenin may be related to the relatively weak binding affinity. In the β-catenin–E-cadherin interactions, phosphorylation of E-cadherin seems to be essential for the affinity of the β-catenin–E-cadherin complex and cell adhesiveness (Lickert *et al*., 2000).

Implication for other FERM-like domains

FERM-like domains have been found in other cross-linker proteins such as the neurofibromatosis type 2 tumor-suppressor gene product, which is also referred to as

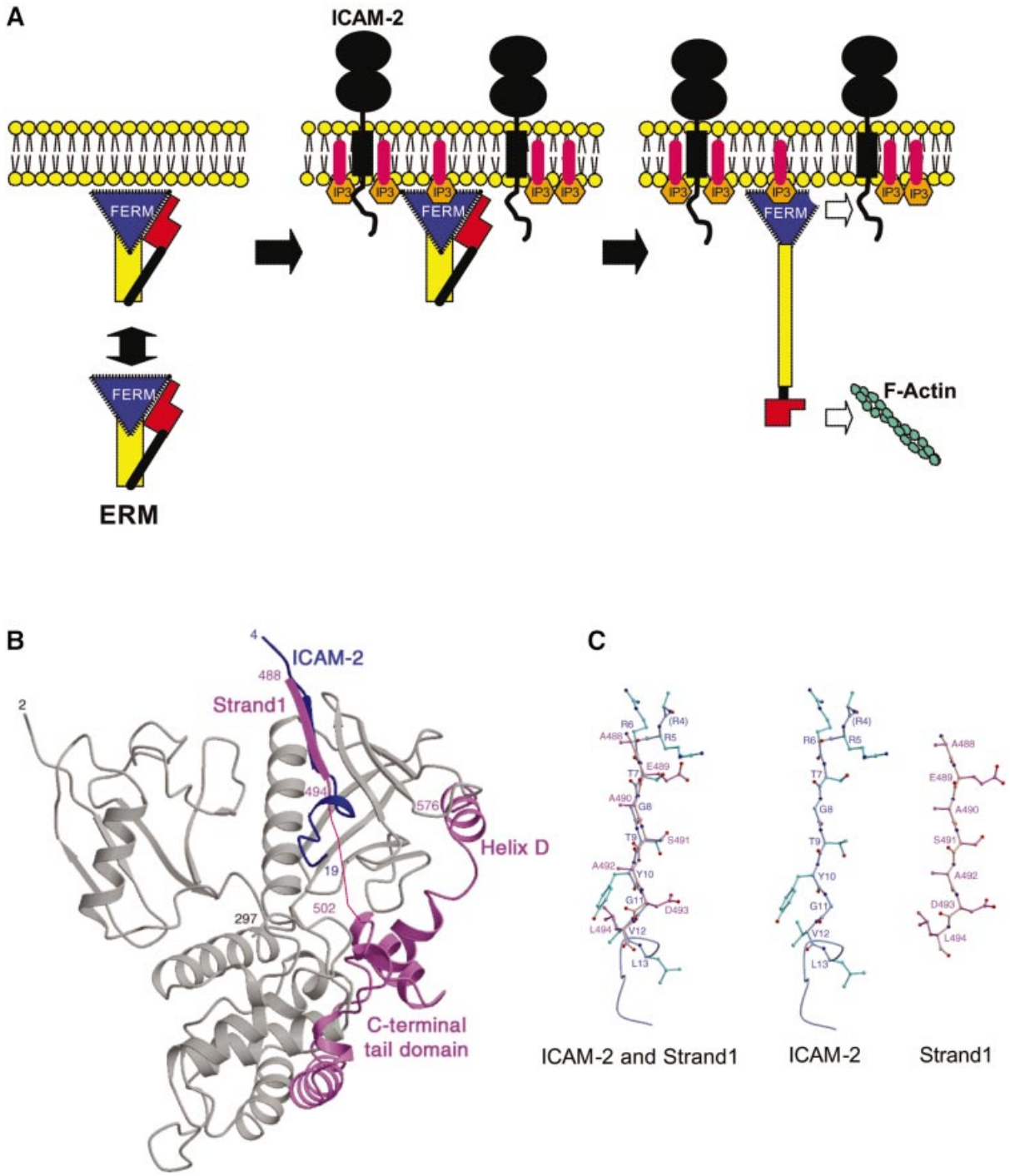

Fig. 4. Membrane-targeting and unmasking of ERM proteins. (**A**) Model of ERM proteins bound to both PIP2 in a membrane and the ICAM-2 cytoplasmic tail. The N-terminal FERM, the central helical and the C-terminal tail domains are shown with a triangle in blue, a rectangle in yellow and a block in red, respectively. ERM proteins partition between the cell cortex and cytosol. ICAM-2 in plasma membranes colocalized with PIP2. PIP2 molecules recruit masked ERM proteins from the cytosol to plasma membranes and unmask the masked ERM proteins for subsequent binding to the cytoplasmic tails of adhesion molecules such as ICAM-2 and actin filaments. (**B**) Comparison of the FERM–ICAM-2 complex with the masked form of moesin. Superposition of the C-terminal tail domain (pink) in the moesin FERM domain–C-tail complex on the radixin FERM domain (gray) bound to the ICAM-2 peptide (blue). (**C**) Comparison of the β-strand of ICAM-2 (blue green) and strand 1 of the moesin C-terminal tail domain (pink).

merlin/schwannomin (Rouleau *et al*., 1993; Troffater *et al*., 1993), talin, which binds integrin-β (Calderwood *et al*., 1999; Patil *et al*., 1999), protein tyrosine phosphatases (PTPs) such as FAP-1 (PTP-BAS), which associates with Fas (Sato *et al*., 1995), focal adhesion kinase (FAK) (Schultz *et al*., 1998) and membrane-associated unconventional myosins such as myosins VIIa and X (Chishti *et al*., 1998). Moreover, FERM domains have been found in the Janus kinase (JAK) family non-receptor tyrosine kinases that bind interferon receptors (Girault *et al*., 1999). Of these proteins, the merlin FERM domain exhibits a relatively high (64%) sequence identity against those of

ERM proteins and seems to exhibit a similar specificity in recognition of adhesion molecules. In fact, recently crystallographic studies have revealed the merlin FERM domain structure that closely resembles those of radixin and moesin (Kang *et al*., 2002; Shimizu *et al*., 2002). In contrast to the high sequence identity of merlin, the identities of band 4.1 (27%), tailin (24%) and PTPs (~25–33%) are low, and those of FAK and JAK extremely low. Therefore, it remains unclear whether all of these proteins bind their target receptors/adhesion molecules using a PTB-like subdomain C. The band 4.1 protein binds anion exchanger/band 3 as well as glycophorin C (Jons and Drenckhahn, 1992). Recently, the tyrosine phosphatase PTPD1, which is one of the tyrosine phosphatases possessing a FERM-like domain, has been found to bind a new kinesin-like motor protein, KIF1C (Dorner *et al*., 1998). Our close inspection of the amino acid sequences at the possible binding regions of these proteins suggests that they may have variants of the FERM-binding motif RxxTYxVxxA for binding to the FERM or FERM-like domains (Figure 3B).

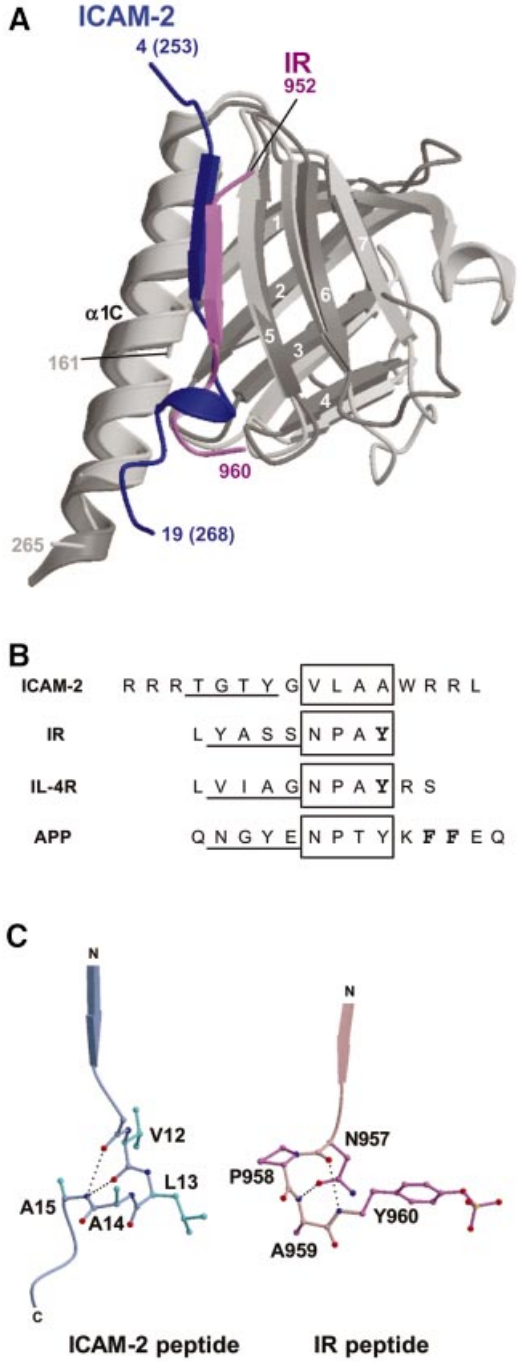

Fig. 5. Comparison of the FERM–ICAM-2 complex with the related PTB–peptide complexes. (**A**) Superposition of the radixin FERM subdomain C (gray) bound to the ICAM-2 tail (blue) on the IRS-1 PTB domain (light gray) bound to the IR peptide (pink). (**B**) Peptide alignment based on the superimposed complex structures. The β-strands formed in the complex formations are underlined. The 3_{10} helix in ICAM-2 and the NPxY motif sequences in the PTB domain-binding (IR, IL-4R and APP) peptides are boxed. The phosphotyrosine residues are in bold in the IR and IL-4R peptides. In the APP peptide, two Phe residues anchoring the peptide to the X11 PTB domain are also in bold. (**C**) Comparison of the 3_{10} helix in the ICAM-2 peptide bound to the radixin FERM domain with the β-turn of the NPxY motif in the IR peptide bound to the IRS-1 PTB domain. The intra-peptide hydrogen bonds are shown as dotted lines.

Conclusion

The present work reveals the peptide-binding mode of the radixin FERM domain, which uses the PTB-like subdomain C for recognition of the FERM-binding motif RxxTYxVxxA through a β–β association and most likely the acidic groove between subdomains B and C for electrostatic interactions. Basic residues at the N-terminal flanking region of the motif may not be essential for FERM binding, but may be important for possible interactions with acidic lipid components such as PIP2. The ICAM-2 peptide forms a short 3_{10} helix instead of the

Table III. Crystallographic analysis of the radixin FERM domain–ICAM-2 complex

Intensity data	
Resolution (Å)	2.40
Reflections	
measured	599 708
unique	23 153
Completeness (%)[a]	100.0/100.0
R_{sym}[b] (%)[a]	7.1/13.7
Mean I/σ[a]	6.0/5.2
Refinement	
Resolution range (Å)	15.0–2.40
Number of residues	332
protein	316
peptide	16
Atoms included	2998
protein	2618
peptide	116
water	264
R_{cryst} factor/R_{free} factor (%)[c]	22.9/24.0
Mean B factor (Å^2)	49.4
protein	48.9
peptide	59.2
R.m.s. deviations[d]	0.008 Å, 1.350°, 1.182°

[a]Each pair of values are for overall/outer shell. The resolution ranges of their outer shells are 2.53–2.40 Å.
[b]$R_{sym} = \Sigma|I - \langle I\rangle| / \Sigma I$; calculated for all data.
[c]R_{cryst} and $R_{free} = \Sigma||F_o| - |F_c|| / \Sigma|F_o|$, where the free reflections (10% of the total used) were held aside for R_{free} throughout refinement.
[d]The three values are for bond lengths, bond angles and impropers, respectively.

β-turn formed by the NPxY motif that is the signature sequence recognized by 'classical' PTB domains. Specific contacts have been identified on the complex structure and also been verified using a quantitative binding assay. These contacts, as well as electrostatic interactions involving the C-terminal basic region, whose structure was not specified in this study, collectively achieve high affinity and specificity.

Materials and methods

Protein preparation and binding studies

The FERM domain (1–310 residues) of mouse radixin was expressed as a fusion protein with GST in *Escherichia coli* and purified by methods described previously (Hamada *et al*., 2001). For binding studies, SPR measurements were carried out on a BIAcore Biosensor instrument (BIAcore 3000, Pharmacia Biosensor). Biotinylated polypeptides of the juxtamembrane regions of the adhesion molecules, which were synthesized by a Fmoc-based strategy with standard side-chain protecting groups and were purified by reverse phase HPLC, were purchased from Sawady Technology (Tokyo, Japan). The peptide was coupled via the N-terminal biotin moiety to streptavidin-coated sensor chip (sensor chip SA BIAcore AB). The radixin FERM domain (~0.1–1 μM) was injected into both the peptide-linked and non-linked sensor chips for correction of background signals. All binding experiments were performed at 25°C with a flow rate of 10 μl/min in buffer (10 mM HEPES pH 7.4, 150 mM NaCl, 1 mM EDTA, 1 mM DTT and 0.05% surfactant P20). The kinetic parameters were evaluated using the BIA evaluation software (Pharmacia). The K_d values were obtained by averaging of at least three independent measurements and are summarized in Table I.

Crystallization and data collection

For crystallization, the purified protein was mixed with the equimolar 28-residue ICAM-2 peptide and concentrated to 20 mg/ml (0.54 mM). The complex crystals were obtained from a 0.27 mM protein/peptide solution with 1:1 stoichiometry containing 50 mM Mes-Na (pH 6.0), 2% polyethylene glycol 6000 (PEG6K), 130 mM NaCl and 0.4 mM DTT at 4°C. MALDI-TOF mass spectroscopy of an aliquot in which crystals were dissolved indicated that the crystals contained the FERM domain and the ICAM-2 peptide (Hamada *et al*., 2001).

All diffraction data were collected from crystals flash-frozen to 100 K after cryoprotection in a solution containing 7% PEG6K, 35% glycerol and 50 mM Mes-Na buffer. Crystals belonged to space group $P3_121$, which was determined by the following structure analysis, with unit cell parameters, $a = b = 100.44$ Å, $c = 99.49$ Å, $\gamma = 120°$. A 2.4-Å data set was collected using a charge-coupled area detector (Mar CCD) installed on the beam line BL41XU at the SPring-8 synchrotron facility, Harima, Japan. The wavelength was set to 1.00 Å with a crystal-to-detector distance of 160 mm. The data were collected from three crystals with angular ranges of 180° with step sizes of 1° for an exposure time of 3 s. Intensity data were processed using the programs DENZO and SCALEPACK (Otwinowski and Minor, 1997) or DPS-Mosfilm (Rossmann and van Beek, 1999). Two data sets were merged into one set of data for structure determination (Table III).

Structure determination and refinement

The initial phases were calculated by molecular replacement using a search model based on the free state structure of the radixin FERM domain (Hamada *et al*., 2000). Unambiguous rotation and translation solutions were obtained from several searches using different ranges of intensity data and integration radii with the program AMoRe (Navaza, 1994). After rigid-body refinements of the search model performed with the program CNS (Brünger *et al*., 1998), the phases were improved by solvent flattening and histogram matching using Solomon (Abrahams and Leslie, 1996). The resultant initial map shows clear electron densities for most of the FERM domain and the peptide. An initial model of the peptide was built into the electron density map using the graphics program O (Jones *et al*., 1991) as well as rebuilding part of the FERM domain. The model was refined by the method of simulated annealing using CNS (Brünger *et al*., 1998). After several cycles of rebuilding and refinement, the model was refined to an R value of 22.9% (free R value of 24.0%) for intensity data at a 2.4 Å resolution. The current model includes 316 residues of the protein (six residues arising from the vector), 16 residues of peptide and 264 water molecules. The stereochemical quality of the model was monitored using the program PROCHECK (Laskowski *et al*., 1993).

In the peptide model, the side chains of Arg4, Arg17, Arg18 and Leu19 were poorly defined and in the current structure are replaced with alanines. No model was built for the three N-terminal and nine C-terminal residues of the peptide, which are poorly defined in the current map. In the protein model, the side chains of Pro2 and Lys3 were poorly defined and in the current structure are replaced with alanines. Asp252 is in disallowed main-chain torsion angle regions.

Ribbon representations of the main-chain folding of the molecule were drawn using the program Molscript (Kraulis, 1991), while molecular surface representations were drawn using the program GRASP (Nicholls *et al*., 1991).

Acknowledgements

We thank Dr S.E.Shoelson (Harvard Medical School, Boston) for providing the coordinates of the IR–IRS-1 PTB domain complex. We also thank Drs K.Okada and M.Kawamoto for their technical assistance in data collection at the SPring-8 Facility, Harima. This work was supported by Grants-in-Aid for Scientific Research to T.H. (12490024, 10359003) and Grants-in-Aid for Scientific Research on Priority Area to S.T. and T.H. (10179103-4) from the MESSC of Japan. K.H. was supported by a research fellowship for Young Scientists from JSPS. T.H. is a member of the TARA project of Tsukuba University. Coordinates for the complex have been deposited in the Protein Data Bank of the Research Collaboratory for Structural Bioinformatics under accession No. 1J19.

References

Abrahams,J.P. and Leslie,A.G.W. (1996) Methods used in the structure determination of bovine mitochondrial F_1 ATPase. *Acta Crystallogr. D*, **52**, 30–42.

Allenspach,E.J. *et al*. (2001) ERM-dependent movement of CD43 defines a novel protein complex distal to the immunological synapse. *Immunity*, **15**, 739–750.

Amieva,M.R. and Furthmayr,H. (1995) Subcellular localization of moesin in dynamic filopodia, retraction fibers and other structures involved in substrate exploration, attachment and cell–cell contacts. *Exp. Cell Res.*, **219**, 180–196.

Andreoli,C., Martin,M., Le Borgne,R., Reggio,H. and Mangeat,P. (1994) Ezrin has properties to self-associate at the plasma membrane. *J. Cell Sci.*, **107**, 2509–2521.

Arpin,M., Algrain,M. and Louvard,D. (1994) Membrane–actin microfilament connections: an increasing diversity of players related to band 4.1. *Curr. Opin. Cell Biol.*, **6**, 136–141.

Barreiro,O., Yánez-Mó,M., Serrador,J.M., Montoya,M.C., Vicente-Manzanares,M., Tejedor,R., Furthmayr,H. and Sánchez-Madrid,F. (2002) Dynamic interaction of VCAM-1 and ICAM-1 with moesin and ezrin in a novel endothelial docking structure for adherent leukocytes. *J. Cell Biol.*, **157**, 1233–1245.

Barret,C., Roy,C., Montcourrier,P., Mangeat,P. and Niggli,V. (2000) Mutagenesis of the phosphatidylinositol 4,5-bisphosphate (PIP_2) binding site in the NH_2-terminal domain of ezrin correlates with its altered cellular distribution. *J. Cell Biol.*, **151**, 1067–1080.

Bretscher,A. (1999) Regulation of cortical structure by the ezrin–radixin–moesin protein family. *Curr. Opin. Cell Biol.*, **11**, 109–116.

Bretscher,A., Chambers,D., Nguyen,R. and Reczek,D. (2000) ERM-Merlin and EBP50 protein families in plasma membrane organization and function. *Annu. Rev. Cell. Dev. Biol.*, **16**, 113–143.

Brünger,A.T. *et al*. (1998) Crystallography and NMR system: a new software suite for macromolecular structure determination. *Acta Crystallogr. D*, **54**, 905–921.

Calderwood,D.A., Zent,R., Grant,R., Rees,D.J., Hynes,R.O. and Ginsberg,M.H. (1999) The Talin head domain binds to integrin β subunit cytoplasmic tails and regulates integrin activation. *J. Biol. Chem.*, **274**, 28071–28074.

Chishti,A.H. *et al*. (1998) The FERM domain: a unique module involved in the linkage of cytoplasmic proteins to the membrane. *Trends Biochem. Sci.*, **23**, 281–282.

Delon,J., Kaibuchi,K. and Germain,R.N. (2001) Exclusion of CD43 from the immunological synapse is mediated by phosphorylation-regulated relocation of the cytoskeletal adaptor moesin. *Immunity*, **15**, 691–701.

Dickson,T.C., Mintz,C.D., Benson,D.L. and Salton,S.R.J. (2002)

Functional binding interaction identified between the axonal CAM L1 and members of the ERM family. *J. Cell Biol.*, **157**, 1105–1112.

Dhe-Paganon,S., Ottinger,E.A., Nolte,R.T., Eck,M.J. and Shoelson,S.E. (1999) Crystal structure of the pleckstrin homology–phosphotyrosine binding (PH–PTB) targeting region of insulin receptor substrate 1. *Proc. Natl Acad. Sci. USA*, **96**, 8378–8383.

Dorner,C., Ciossek,T., Müller,S., Møller,N.P.H., Ullrich,A. and Lammers,R. (1998) Characterization of KIF1C, a new kinesin-like protein involved in vesicle transport from the Golgi apparatus to the endoplasmic reticulum. *J. Biol. Chem.*, **273**, 20267–20275.

Eck,M.J., Dhe-Paganon,S., Trüb,T., Nolte,R.T. and Shoelson,S.E. (1996) Structure of the IRS-1 PTB domain bound to the juxtamembrane region of the insulin receptor. *Cell*, **85**, 695–705.

Franck,Z., Gary,R. and Bretscher,A. (1993) Moesin, like ezrin, colocalizes with actin in the cortical cytoskeleton in cultured cells, but its expression is more variable. *J. Cell Sci.*, **105**, 219–231.

Gary,R. and Bretscher,A. (1995) Ezrin self-association involves binding of an N-terminal domain to a normally masked C-terminal domain that includes the F-actin binding site. *Mol. Biol. Cell*, **6**, 1061–1075.

Girault,J.A., Labesse.G., Mornon.J.P. and Callebaut,I. (1999) The N-termini of FAK and JAKs contain divergent band 4.1 domains. *Trends Biochem. Sci.*, **24**, 54–57.

Hamada,K., Shimizu,T., Matsui,T., Tsukita,Sh., Tsukita,Sa. and Hakoshima,T. (2000) Structural basis of the membrane-targeting and unmasking mechanisms of the radixin FERM domain. *EMBO J.*, **19**, 4449–4462.

Hamada,K., Shimizu,T., Matsui,T., Tsukita,Sh., Tsukita,Sa. and Hakoshima,T. (2001) Crystallographic characterization of the radixin FERM domain bound to the cytosolic tail of the adhesion molecule ICAM-2. *Acta Crystallogr. D*, **57**, 891–892.

Heiska,L., Alfthan,K., Grönholm,M., Vilja,P., Vaheri,A. and Carpén,O. (1998) Association of ezrin with intercellular adhesion molecule-1 and -2 (ICAM-1 and ICAM-2). Regulation by phosphatidylinositol 4,5-bisphosphate. *J. Biol. Chem.*, **273**, 21893–21900.

Helander,T.S., Carpen,O., Turunen,O., Kovanen,P.E., Vaheri,A. and Timonen,T. (1996) ICAM-2 redistributed by ezrin as a target for killer cells. *Nature*, **382**, 265–268.

Hirao,M., Sato,N., Kondo,T., Yonemura,S., Monden,M., Sasaki,T., Takai,Y., Tsukita,Sh. and Tsukita,Sa. (1996) Regulation mechanism of ERM (ezrin/radixin/moesin) protein/plasma membrane association: possible involvement of phosphatidylinositol turnover and Rho-dependent signaling pathway. *J. Cell Biol.*, **135**, 37–51.

Huber,A.H. and Weis,W.I. (2001) The structure of the β-catenin/E-cadherin complex and the molecular basis of diverse ligand recognition by β-catenin. *Cell*, **105**, 391–402.

Jones,T.A., Zou,J.-Y., Cowan,S.W. and Kjeldgaard,M. (1991) Improved methods for building protein models in electron density maps and the location of errors in these models. *Acta Crystallogr. A*, **47**, 110–119.

Jons,T. and Drenckhahn,D. (1992) Identification of the binding interface involved in linkage of cytoskeletal protein 4.1 to the erythrocyte anion exchanger. *EMBO J.*, **11**, 2863–2867.

Kang,B.S., Cooper,D.R., Devedjiev,Y., Derewenda,U. and Derewenda,Z.S. (2002) The structure of the FERM domain of merlin, the neurofibromatosis type 2 gene product. *Acta Crystallogr. D*, **58**, 381–391.

Kraulis,P.J. (1991) MOLSCRIPT—a program to produce both detailed and schematic plots of protein structures. *J. Appl. Crystallogr.*, **24**, 946–950.

Laskowski,R.A., MacArthur,M.W., Moss,D.S. and Thornton,J.M. (1993) PROCHECK: a program to check the stereochemical quality of protein structures. *J. Appl. Crystallogr.*, **26**, 283–291.

Li,S.C., Zwahlen,C., Vincent,S.J., McGlade,C.J., Kay,L.E., Pawson,T. and Forman-Kay,J.D. (1998) Structure of a Numb PTB domain–peptide complex suggests a basis for diverse binding specificity. *Nat. Struct. Biol.*, **5**, 1075–1083.

Lickert,H., Bauer,A., Kemler,R. and Stappert,J. (2000) Casein kinase II phosphorylation of E-cadherin increases E-cadherin/β-catenin interaction and strengthens cell–cell adhesion. *J. Biol. Chem.*, **275**, 5090–5095.

Magendantz,M., Henry,M.D., Lander,A. and Solomon,F. (1995) Interdomain interactions of radixin *in vitro*. *J. Biol. Chem.*, **270**, 25324–25327.

Mangeat,P., Roy,C. and Martin,M. (1999) ERM proteins in cell adhesion and membrane dynamics. *Trends Cell Biol.*, **9**, 187–192.

Nakamura,F., Huang,L., Pestonjamasp,K., Luna,E.J. and Furthmayr,H. (1999) Regulation of F-actin binding to platelet moesin *in vitro* by both phosphorylation of threonine 558 and polyphosphatidylinositides. *Mol. Biol. Cell*, **10**, 2669–2685.

Navaza,J. (1994) AMoRe: an automated package for molecular replacement. *Acta Crystallogr. A*, **50**, 157–163.

Nicholls,A., Sharp,K.A. and Honig,B. (1991) Protein folding and association: insights from the interfacial and thermodynamic properties of hydrocarbons. *Proteins*, **11**, 281–296.

Niggli,V., Andréoli,C., Roy,C. and Mangeat,P. (1995) Identification of a phosphatidylinositol-4,5-bisphosphate-binding domain in the N-terminal region of ezrin. *FEBS Lett.*, **376**, 172–176.

Otwinowski,Z. and Minor,W. (1997) Processing of X-ray diffraction data collected in oscillation mode. *Methods Enzymol.*, **276**, 307–326.

Patil,S., Jedsadayanmata,A., Wencel-Drake,J.D., Wang,W., Knezevic,I. and Lam,S.C. (1999) Identification of a talin-binding site in the integrin β_3 subunit distinct from the NPLY regulatory motif of post-ligand binding functions. The talin N-terminal head domain interacts with the membrane-proximal region of the β_3 cytoplasmic tail. *J. Biol. Chem.*, **274**, 28575–28583.

Pearson,M.A., Reczek,D., Bretscher,A. and Karplus,P.A. (2000) Structure of the ERM protein moesin reveals the FERM domain fold masked by an extended actin binding tail domain. *Cell*, **101**, 259–270.

Rossmann,M.G. and van Beek,C.G. (1999) Data processing. *Acta Crystallogr. D*, **55**, 1631–1640.

Rouleau,G.A. *et al*. (1993) Alteration in a new gene encoding a putative membrane-organizing protein causes neuro-fibromatosis type 2. *Nature*, **363**, 515–521.

Sato,N., Yonemura,S., Obinata,T., Tsukita,Sa. and Tsukita,Sh. (1991) Radixin, a barbed end-capping actin-modulating protein, is concentrated at the cleavage furrow during cytokinesis. *J. Cell Biol.*, **113**, 321–330.

Sato,N., Funayama,N., Nagafuchi,A., Yonemura,S., Tsukita.Sa. and Tsukita,Sh. (1992) A gene family consisting of ezrin, radixin and moesin. Its specific localization at actin filament/plasma membrane association sites. *J. Cell Sci.*, **103**, 131–143.

Sato,T., Irie,S., Kitada,S. and Reed,J.C. (1995) FAP-1: a protein tyrosine phosphatase that associates with Fas. *Science*, **268**, 411–415.

Schultz,J., Milpetz,F., Bork,P. and Ponting,C.P. (1998) SMART, a simple modular architecture research tool: identification of signaling domains. *Proc. Natl Acad. Sci. USA*, **95**, 5857–5864.

Serrador,J.M., Alonso-Lebrero,J.L., del Pozo,M.A., Furthmayr,H., Schwartz-Albiez,R., Calvo,J., Lozano,F. and Sánchez-Madrid,F. (1997) Moesin interacts with the cytoplasmic region of intercellular adhesion molecule-3 and is redistributed to the uropod of T lymphocytes during cell polarization. *J. Cell Biol.*, **138**, 1409–1423.

Serrador,J.M. *et al*. (1998) CD43 interacts with moesin and ezrin and regulates its redistribution to the uropods of T lymphocytes at the cell–cell contacts. *Blood*, **91**, 4632–4644.

Shaw,A.S. (2001) FERMing up the synapse. *Immunity*, **15**, 683–686.

Shimizu,T., Seto,A., Maita,N., Hamada,K., Tsukita,Sh., Tsukita,Sa. and Hakoshima,T. (2002) Structural basis or the neurofibromatosis type 2: crystal structure of the Merlin FERM domain. *J. Biol. Chem.*, **277**, 10332–10336.

Takeuchi,K., Kawashima,A., Nagafuchi,A. and Tsukita,Sh. (1994) Structural diversity of band 4.1 superfamily members. *J. Cell Sci.*, **107**, 1921–1928.

Trofatter,J.A. *et al*. (1993) A novel moesin-, ezrin-, radixin-like gene is a candidate for the neurofibromatosis 2 tumor suppressor. *Cell*, **72**, 791–800.

Tsukita,Sa., Oishi,K., Sato,N., Sagara,J., Kawai,A. and Tsukita,Sh. (1994) ERM family members as molecular linkers between the cell surface glycoprotein CD44 and actin-based cytoskeletons. *J. Cell Biol.*, **126**, 391–401.

Tsukita,Sa. and Yonemura,S. (1999) Cortical actin organization: lessons from ERM (Ezrin/Radixin/Moesin) proteins. *J. Biol. Chem.*, **274**, 34507–34510.

Turunen,O., Wahlstrom,T. and Vaheri,A. (1994) Ezrin has a COOH-terminal actin-binding site that is conserved in the ezrin protein family. *J. Cell Biol.*, **126**, 1445–1453.

Yonemura,S., Nagafuchi.A., Sato,N. and Tsukita,Sh. (1993) Concentration of an integral membrane protein, CD43 (leukosialin, sialophorin), in the cleavage furrow through the interaction of its cytoplasmic domain with actin-based cytoskeletons. *J. Cell Biol.*, **120**, 437–449.

Yonemura,S., Hirao,M., Doi,Y., Takahashi,N., Kondo,T., Tsukita,Sa. and Tsukita,Sh. (1998) Ezrin/Radixin/Moesin (ERM) proteins bind to a positively charged amino acid cluster in the juxta-membrane

cytoplasmic domain of CD44, CD43 and ICAM-2. *J. Cell Biol.*, **140**, 885–895.

Yonemura,S., Matsui,T., Tsukita,Sh. and Tsukita,Sa. (2002) Rho-dependent and -independent activation mechanisms of ezrin/radixin/moesin proteins: an essential role for polyphosphoinositides *in vivo*. *J. Cell Sci.*, **115**, 2569–2580.

Zhang,Z., Lee,C.H., Mandiyan,V., Borg,J.P., Margolis,B., Schlessinger,J. and Kuriyan,J. (1997) Sequence-specific recognition of the internalization motif of the Alzheimer's amyloid precursor protein by the X11 PTB domain. *EMBO J.*, **16**, 6141–6150.

Received September 5, 2002; revised November 25, 2002; accepted November 26, 2002